Therapeutic inhibitory RNA in head and neck cancer via functional targeted lipid nanoparticles

Liyona Kampel, Meir Goldsmith, Srinivas Ramishetti, Nuphar Veiga, Daniel Rosenblum, Anna Gutkin, Sushmita Chatterjee, Moran Penn, Galya Lerman, Dan Peer, Nidal Muhanna

PII: S0168-3659(21)00377-1

DOI: https://doi.org/10.1016/j.jconrel.2021.07.034

Reference: COREL 11038

To appear in: *Journal of Controlled Release*

Received date: 20 March 2021

Revised date: 7 July 2021

Accepted date: 19 July 2021

Please cite this article as: L. Kampel, M. Goldsmith, S. Ramishetti, et al., Therapeutic inhibitory RNA in head and neck cancer via functional targeted lipid nanoparticles, *Journal of Controlled Release* (2021), https://doi.org/10.1016/j.jconrel.2021.07.034

Therapeutic Inhibitory RNA in Head and Neck Cancer *via* Functional Targeted Lipid Nanoparticles

Liyona Kampel[1,2,3,4,5,6,7], Meir Goldsmith[3,4,5,6,7], Srinivas Ramishetti[3,4,5,6,7], Nuphar Veiga[3,4,5,6,7], Daniel Rosenblum[3,4,5,6,7], Anna Gutkin[3,4,5,6,7], Sushmita Chatterjee[3,4,5,6,7], Moran Penn[1], Galya Lerman[1], Dan Peer[3,4,5,6,7,*] and Nidal Muhanna[1,2*]

1. The Head and Neck Cancer Research Laboratory, Tel-Aviv Sourasky Medical Center, affiliated to the Sackler School of Medicine, Tel-Aviv University, Tel-Aviv 6423906, Israel.
2. The Department of Otolaryngology, Head and Neck Surgery and Maxillofacial Surgery, Tel-Aviv Sourasky Medical Center, affiliated to the Sackler School of Medicine, Tel-Aviv University, Tel-Aviv 6423906, Israel.
3. Laboratory of Precision NanoMedicine, Tel Aviv University, Tel Aviv 69978, Israel
4. Shmunis School of Biomedicine and Cancer Research, George S. Wise Faculty of Life Sciences, Tel Aviv University, Tel Aviv 69978, Israel
5. Department of Materials Sciences & Engineering, Iby and Aladar Fleischman Faculty of Engineering, Tel Aviv University, Tel Aviv 69978, Israel
6. Center for Nanoscience and Nanotechnology, Tel Aviv University, Tel Aviv 69978, Israel
7. Cancer Biology Research Center, Tel Aviv University, Tel Aviv 69978, Israel

*Corresponding Authors:

D.P. peer@tauex.tau.ac.il

N.M. nmuhanna@gmail.com

Abstract

Currently there are no specific therapies addressing the distinctive biology of human papillomavirus (HPV)-induced cancer approved for clinical use. Short interfering RNA (siRNA) has much potential for therapeutic manipulation of HPV E6/E7 oncoproteins. Lipid-based nanoparticles (LNPs) can be utilized for systemic transportation and delivery of siRNA at target site. We recently developed a recombinant protein linker that enables uniform conjugation of targeting antibodies to the LNPs. Herein, we demonstrate the therapeutic efficacy of anti-E6/E7 siRNA delivered *via* targeted LNPs (tLNPs) in a xenograft HPV-positive tumor model. We show that anti-epidermal growth factor receptor (EGFR) antibodies, anchored to the LNPs as targeting moieties, facilitate cargo delivery but also mediate anti-tumor activity. Treatment with siE6 *via* tLNPs resulted in 50% greater reduction of tumor volume compared to treatment with siControl encapsulated in iso-LNPs (coated with isotype control antibodies). We demonstrate superior suppression of HPV oncogenes and higher induction of apoptosis by the tLNPs both *in vitro* and *in vivo*. Altogether, the coupling of inhibitory siE6 with anti-EGFR antibodies, that further elicited anti-tumor effects, successfully restricted tumor progression. This system that combines potent siRNA and therapeutically functional tLNPs can be modulated against various cancer models.

Keywords: lipid-based nanoparticle, siRNA, targeting, head and neck cancer, HPV

1. Introduction

Head and neck cancer (HNC) is the sixth leading cause of cancer worldwide, with approximately 600,000 newly diagnosed cases each year.[1] The rising incidence of human papillomavirus (HPV) infections has led to a notable increase in HPV-associated HNC diagnosis, especially among young adults.[2–4] No HPV-specific therapies are currently available, and existing oncologic management protocols are mostly limited to cytotoxic chemoradiation that detrimentally affects quality of life. The oncogenic function of HPV has been extensively investigated during the past decades in search of more precise therapeutic targets. The viral proteins, E6 and E7, were found to play an essential role in virus replication and malignant transformation.[5,6] E6 was shown to promote ubiquitin-mediated p53 degradation,[7] and E7 was shown to modulate the function of retinoblastoma family of proteins (pRb, p107, and p130), leading to uncontrolled proliferation.[5] E7 can also induce genome instability and genetic alternations, and the expression of both oncoproteins is considered pivotal for maintaining the malignant phenotype.[6] Genetic manipulation of these key targets by means of various strategies has been applied in pre-clinical models. Short interfering RNA (siRNA) against HPV E6 and E7 was shown to successfully induce apoptosis of HPV-positive cervical and oropharyngeal cancer cell-lines.[8,9] It was also demonstrated that intra-tumoral injection of siRNA targeting HPV E6 and E7 can elicit tumor growth inhibition in tumor-bearing mice.[10,11]

Despite its promising potential, the clinical translation of siRNA-based drugs for HPV-induced cancer as well as for solid tumors in general has been hindered by mechanical and physiological barriers related to systemic administration. One major obstacle is the instability of naked siRNA in circulation due to immune system activation, rapid degradation and elimination by the reticuloendothelial system (RES).[12,13] In addition, upon reaching the target cell, membrane penetration is limited by siRNA negative charge and large molecular

weight (~13 kDa).[14] Versatile delivery vehicles were designed to overcome these barriers, and lipid-nanoparticles (LNPs) became one of the leading technologies for *in vivo* systemic siRNA transportation.[15,16] These nanocarriers for siRNAs, however, have shown only modest success, and very few formulations have entered clinical trials on patients with advanced or refractory solid tumors.[17–19] The complex microscopic architecture of solid tumors poses major challenges for sufficient delivery of nanocarriers.[20,21] In most cases, less than 1% of an intravenously injected dose of the nanoparticles is successfully delivered into a solid tumor.[22]

Structural modifications of the LNPs can be applied to resist circulatory and tumor-related barriers and to achieve a better therapeutic index of the nanocarriers. Active targeting is one of the strategies utilized to improve therapeutic efficacy by enhancing specific target-cell uptake while reducing off-target side effects.[23–25] In HNC, the Erb family of receptor tyrosine kinases (RTKs), which is ubiquitously expressed on most cancers of epithelial origin,[26] provides excellent targetable surface markers. In addition to excessive expression, inappropriate activation of the Erb receptors was also shown to promote tumorigenesis.[27] Anticancer therapy based on epidermal growth factor receptor (EGFR) blockade has been validated and approved for clinical use in patients with advanced HNC.[28,29]

In this study, we tested the utility of siRNA against HPV-E6/E7 encapsulated in LNPs as a specific therapeutic modality for HPV-induced HNC. We hypothesized that antibodies against EGFR can be used to actively target the LNPs into HNC cells, adding another layer of specificity and at the same time providing additional therapeutic effect, by modulating fundamental intracellular pathways initiated by EGFR activation. To test this hypothesis, we have devised targeted LNPs (tLNPs) by means of our recently designed modular targeting

platform, named ASSET (Anchored Secondary scFv Enabling Targeting), [30] that enables anchoring of monoclonal antibodies (mAbs) to the LNP surface. This technology is based on biological conjugation of a lipoprotein, purified from E.coli that self assembles with the LNPs surface and interacts with the mAb Fc domain to mediate efficient binding to target receptor. We established a xenograft HPV-positive HNC mouse model and showed that employing anti-EGFR mAbs for targeting not only enhances *in vivo* LNPs uptake specifically in cancer cells, but also confers therapeutic advantage by stimulating anti-tumor activity. The use of tLNPs boosted the therapeutic efficacy of the anti-HPV siRNA, as demonstrated by augmented induction of apoptosis *in vitro* and enhanced tumor growth inhibition *in vivo,* compared to LNPs coated with isotype control mAbs (iso-LNPs). We now present pre-clinical evidence for successful tumor growth inhibition in a solid cancer model achieved by siRNA administered systemically *via* EGFR-targeting LNPs. Ultimately, this treatment strategy that combines potent anti-HPV siRNA with functional anti-EGFR tLNPs holds great promise for a virus-specific treatment for HPV-induced cancer, and ultimately for many other malignant diseases in the era of precision medicine.

2. Materials and methods

2.1 *Cell culture and cell lines*

FaDu and 2A3 hypopharyngeal carcinoma cell lines (ATCC, USA) and the UMSCC-104 cell line (Millipore, USA) were routinely cultured in Dulbecco's modified eagle's medium (DMEM) (Biological Industries, Israel) supplemented with 10% heat-inactivated fetal bovine serum (FBS), 100μg/ml Penicillin-Streptomycin-Nystatin, 1% L-glutamine (Biological Industries, Israel) and 1% MEM non-essential amino acids supplement (Sigma, USA). The UPCI:SCC090 oropharyngeal carcinoma cell line (ATCC, USA) was cultured in EMEM

(ATCC, USA) supplemented with 10% FBS, 100µg/ml Penicillin-Streptomycin-Nystatin and 1% L-glutamine . Cells were grown and maintained in a humidified incubator at 37 ^{O}C with 5% CO_2. All cells were routinely checked for mycoplasma contamination with the EZ-PCR Mycoplasma Test Kit (Biological Industries, Israel), according to the manufacturer's protocol.

2.2 *siRNA and transfections in vitro*

Chemically modified Dicer-substrate siRNAs against HPV16-E6/E7, scrambled control siRNA, and Cy5-labelled siRNA were synthesized at IDT (Coralville, Iowa, USA) with standard phosphoramidite chemistry and the following sequences: E6-189: Sense rArArUrGrUrGrUrGrUrArCrUrGrCrArArGrCrArArCrArGTT, Antisense rArArCrUrGrUrUrGrCrUrUrGrCrArGrUrArCrArCrArUrUrCrU; E6-586: Sense rGrGrArGrArUrArCrArCrCrUrArCrArUrUrGrCrArUrGrAAT, antisense rArUrUrCrArUrGrCrArArUrGrUrArGrGrUrGrUrArUrCrUrCrCrArU; Scrambled control (NC): sense rCrUrA rArCrG rCrGrA rCrUrA rUrArC rGrCrG rCrArA rUrArU rGrGrU anti-sense rCrArU rArUrU rGrCrG rCrGrU rArUrA rGrUrC rGrCrG rUrUA G**.** Another siRNA against HPV16-E6 was designed as described by Yamato *et al* [31] and purchased from Dharmacon (Colorado, USA) with the following sequence (497): passenger strand 5'-GACCGGUCGAUGUAUGUCUUG-3' guide strand 5'-AGACAUACAUCGACCGGUCCA-3'. Cells at 30-40% confluency in 12-well plates were transfected with siRNA (10μ_M), lipofectamine RNAiMax reagent (Invitrogen, USA) and OptiMEM (Life Technologies, USA), according to the manufacturer's protocol. After 48h and 72h, cells were harvested, RNA was extracted with a NucleoSpin RNA kit (Macherey-Nagel, USA) and cDNA was prepared with a cDNA synthesis kit (Quanta Biosciences, USA). cDNA samples were diluted (1:16) and subjected to PCR amplification with SYBR Green PCR Master Mix (Thermo-Fisher, USA). GAPDH was used as the endogenous

control, and the following primers were used for RT-PCR: E6 forward GAC CCA GAA AGT TAC CAC AGT TA, reverse AGC AAA GTC ATA TAC CTC ACG TC; E7 forward CAA GCA GAA CCG GAC AGA G, reverse CCC ATT AAC AGG TCT TCC AAA GTA; GAPDH forward TGT AGT TGA GGT CAA TGA GGG G, reverse ACA TCG CTC AGA CAC CAT G.

2.2.1 Immunoblotting

At 72h and 96h post-transfection, cells were harvested and whole-cell protein lysates were prepared with radioimmunoprecipitation assay (RIPA) lysis buffer (Sigma-Aldrich, USA) supplemented with a protease and phosphatase inhibitor cocktail (Abcam, USA) on ice. Equal amounts of protein were separated by 12% SDS-PAGE and transferred to a polyvinylidene difluoride membrane (Invitrogen, USA) by means of the iBlot2 gel transfer device (Thermo-Fischer, USA). The membranes were blocked with 5% bovine serum albumin (BSA) in tris-buffered Saline-Tween 20 (TBST) for 1h at room temperature with agitation and then probed by incubation with primary antibodies overnight at 4 ^{O}C. Antibodies for the following proteins were used: P53 (DO-1) (SC-126, Santa Cruz Biotechnology, China), E7 (ab20191, Abcam, Israel) and GAPDH (MAB374, Merck, USA). For visualization of the probed proteins, membranes were incubated with horseradish peroxidase (HRP)–conjugated secondary antibodies for 1h at room temperature and imaged after applying the SuperSignal West Pico PLUS chemiluminescent substrate (ThermoFisher Scientific, USA). Densitometric analyses were performed with ImageJ software.

2.2.2 Cell proliferation assay

Cell viability in response to various treatments was assessed by a cell proliferation kit based on tetrazolium salt (XTT) (Biological Industries, Israel). FaDu, 2A3, UPCI:SCC090 and UMSCC104 cells were seeded in 96-well plates at 7000, 7500, 20,000 or 15,000 cells per

well, respectively. The intensity of the orange-colored reduced product of XTT was measured at 96h post siRNA treatment with a spectrophotometer, following manufacturer's protocol.

2.2.3 Apoptosis assay

FaDu and UMSCC-104 cells were seeded in 12-well plates and treated with the LNPs-siRNA complexes for 96h. Cells were then harvested, washed twice with cold PBS, and resuspended in 100μL of Annexin V binding buffer (Biolegend, USA). The cells were stained with APC-conjugated annexin V antibody (Biolegend, USA) and propidium iodide (Sigma, USA), and analysed by flow cytometry. Data analysis was performed with FlowJo software (Tree Star, Inc., OR, USA).

2.2.4 Immunofluorescence and confocal microscopy

Borosilicate cover glasses (Marienfeld, Germany) were inserted into 24-well plates, and coated with Poly-D-lysine (Sigma Aldrich, USA). Following seeding the cells and administration of treatment, cells were washed with cold PBS, fixed with 4% PFA and incubated overnight with primary antibodies at 4 ^{O}C. The following primary antibodies were used: E7 (ab20191, Abcam Israel), CD44 (Biolegend, clone IM7, USA) and Rb (4H1) (9309S, Cell Signaling, USA). Cells were then washed, incubated with Alexa-Fluor 488-labelled secondary antibodies (ThemoFisher Scientific, USA) for 1h at 4 ^{O}C, after which cover glasses were placed on microscope slides with DAPI-mounting (Moshe Stauber Biotec Applications, Israel). Images were acquired by a LeicaSP8 multiphoton microscope (Leica, USA).

2.3 *Preparation and characterization of lipid-based nanoparticles (LNPs)*

Lipid components of the LNPs included distearoyl-phosphatidylcholine (DSPC), cholesterol, 1,2-dimyristoyl-rac-glycerol-3-methoxypolyethylene glycol-2000 (DMG-PEG), and 1,2-distearoyl-sn-glycero-3-phosphoethanolamine-N-[methoxy (polyethylene glycol)-2000] (DSPE-PEG-Ome) (Avanti Polar Lipids, USA) and the cationic lipid 10 (EA-PIP), designed and synthesized as previously described. [32] Structure of lipid 10 is shown in Supplementary Information Fig S7. LNPs were prepared by the NanoAssembler microfluidic mixing system (Precision NanoSystems, Vancouver, BC) as previously described.[33] Briefly, one volume of lipid mixtures (EA-PIP, DSPC, Chol, DMG-PEG, and DSPE-PEG Ome at 50:10:38:1.5:0.5 mol ratio) in ethanol and three volumes of siRNA (1:16 w/w siRNA to lipid) containing acetate buffer solutions were mixed by a dual syringe pump (model S200, kD Scientific, Holliston, MA) to drive the solutions through the micro mixer at a combined flow rate of 2 mL/min (0.5 mL/min for the ethanol and 1.5 mL/min for the aqueous buffer). The resultant mixture was dialyzed against phosphate buffered saline (PBS) (pH 7.4) for 16 h to remove ethanol. Cy5-labeled particles were prepared with scrambled control siRNA (siNC) and Cy5-labeled siNC in 1:1 ratio. We utilized ASSET technology[30] for the preparation of targeted or iso-LNPs. ASSET (Anchored Secondary scFv Enabling Targeting) is a lipoprotein purified from E.coli in micelles. Briefly, ASSET micelles were incubated with the LNPs for 48h at 4 ^{O}C to allow its incorporation into LNPs. To construct iso-LNPs, rat IgG_{2a} mAbs (clone 2A3, BioXell, USA) were incubated with the ASSET-LNPs conjugates for 30min at 4 ^{O}C (ASSET:mAb in 1:1 weight ratio). tLNPs were assembled in a similar manner, utilizing anti-human EGFR mAbs (MCA1784, clone ICR10, Bio-Rad, USA). The hydrodynamic diameter, size distribution and zeta potential of the LNPs were determined by dynamic light scattering with the Malvern nano ZS Zetasizer (Malvern Instruments Ltd. Worcestershire, UK). Sizes were measured in Dulbecco's phosphate buffered saline (PBS) (Biological Industries, Israel), and pH 7.4 and zeta potential measurements were performed in

double-distilled water (DDW). Transmission electron microscopy (TEM) visualization was performed by a drop of aqueous solution containing the LNPs placed and dried on a carbon-coated copper grid. The preparations were examined in a Jeol TEM 1200EX transmission electron microscope(Jeol, Japan).

2.4 *Xenograft-tumor animal model*

Athymic Foxn1 nude female mice were obtained from Envigo (Envigo, Indiana, USA), housed in a specific pathogen-free animal facility, and maintained according to National Institutes of Health guidelines. All animal protocols were approved by the Tel Aviv University Institutional Animal Care and Usage Committee (Approval number 04-18-019) and were in accordance with current regulations and standards of the Israel Ministry of Health. The xenograft tumor model was established by subcutaneous injection of $0.5x10^6$ UMSCC-104 cells suspended in 100µl of PBS mixed with 100µl Matrigel Matrix (Corning, USA) to the right flanks of 8-week-old mice. Tumor volume was measured with an electronic caliper. Cephalo-caudal length (L) and medio-lateral dimensions (W) were recorded and tumor volume (V) was calculated by the following formula: $V = (L \times W^2) / 2$.

2.4.1 Circulation time, biodistribution and tumor uptake assessment

LNPs encapsulating Cy5-labelled siRNA were injected *via* tail vein at a dose of 1mg siRNA/kg body weight. Blood samples were collected into designated capillary tubes at 15min, 30min, 1h and 2h post-injection. The capillaries were then centrifuged at 2500rpm for 10min at room temperature to separate the plasma from the cellular fraction and imaged by the Maestro imaging system (CRI, Inc., Woburn, MA). The Cy5 fluorescent signal was measured as scaled counts/s/pixels for the region of interest with Spectral analysis Software. To evaluate biodistribution, tumor-bearing mice were randomly assigned to receive intravenous (iv) injection of iso-LNPs or tLNPs encapsulating Cy5-labelled siRNA at a dose

of 1mg siRNA/kg body weight. After 2, 4 and 24h, the mice were anesthetized by isoflurane and whole-body images were taken in the IVIS Spectrum *in vivo* imaging system (PerkinElmer, USA). The mCherry signal was read upon excitation at 570nm and the Cy5 signal was read at 640nm. The mice were then euthanized and the organs and tumors were harvested and imaged by the IVIS imaging system. The intensities of the mCherry and cy5 signals were calculated by marking the regions of interest (ROI), and the total radiant efficiency was measured by the Living image Software version 4.3 (PerkinElmer, USA).

To assess intra-tumoral distribution of LNPs, tumors were harvested 4h post injection and processed for embedding in O.C.T Compound (ThermoFisher Scientific, USA). The O.C.T blocks were cut into 16-µm sections, which were made serially through multiple regions of each tumor. After processing the tissues were incubated overnight with anti-EGFR antibody (R38B1, Cell Signaling Technology, USA). Slides were then washed with PBS and incubated with Alexa-Fluor 488 labelled secondary antibody (ThermoFisher Scientific, USA) for 1h at room temperature, and underwent DAPI immunomounting (Moshe Stauber Biotec Applications, Israel). Dried slides were examined and imaged by a TCS SP8 multiphoton confocal microscope (Leica, USA).

2.4.2 In vivo target genes silencing

Mice were euthanized 72h after the last iv LNPs injection and the tumors were harvested and lysed, and RNA was extracted with an EZ-RNA kit (Biological Industries, Israel) according to the manufacturer's protocol. E6/E7 mRNA expression levels were quantified by RT-PCR as described earlier. Since the baseline expression of E6/E7 in the xenograft tumors was variable, the mRNA expression level was quantified relative to the mean expression level in a group of 5 untreated mice [RQ=1].

2.4.3 Histology, Immunohistochemistry (IHC) and In situ cell death detection assay (TUNEL)

Xenograft tumors harvested 72h after the last LNPs injection were fixed in 10% formalin solution overnight at room temperature, washed and preserved in 70% ethanol solution at 4 ^{O}C. Formalin-fixed paraffin embedded (FFPE) slides were prepared and stained with H&E by the Multistainer Leica ST5020 instrument (Leica, USA). IHC was performed by the Leica BondIII instrument (Leica, USA) and the CDINK2A/P16 antibody (ab108349, Abcam, Israel). The slides were observed under a light microscope (Olympus). TUNEL assay was performed by the *in-situ* cell death detection kit, Fluorescein (Merck, USA) according to the manufacturer protocol. Nuclei were stained with DAPI immuno-mounting. The slides were imaged by the TCS SP8 multiphoton confocal microscope (Leica, USA) and the images were analyzed by ImageJ software.

2.5 *Statistical analysis*

All statistical analyses were performed with GraphPad Prism 8 software (GraphPad Software Inc., La Jolla, CA). A two-sided Student's *t*-test was applied for comparing two experimental groups. ANOVA was applied in experiments with multiple groups. A p-value of less than 0.05 was considered significant.

3. Results

3.1 *HPV-E6/E7 knockdown and induction of cell death*

The oncogenic function of HPV is primarily attributed to the activity of the viral proteins E6 and E7, which are associated with cell cycle dysregulation.[5,6] We investigated whether siRNA-induced knockdown of E6 and E7 effects the viability of HPV-infected tumor cells.

To this end, we obtained three HPV16-positive cell lines, and initially confirmed E6 and E7 expression by RT-PCR and immunoblotting (Fig. 1A). UMSCC-104 and UPCI:SCC090 cell lines were derived from human patients infected with HPV-16, that developed an oral cavity/oropharyngeal tumor, while 2A3 cells originated from FaDu hypopharyngeal cancer cell line (HPV-negative hypopharyngeal tumor), transfected with a plasmid vector expressing HPV16-E6/E7 exclusively. Intrinsic RNAi machinery was engaged to determine whether E6 and E7 knockdown can inhibit the proliferation of HPV-positive HNC cells. E6 and E7 share a single bicistronic pre-mRNA.[34] Various siRNA sequences were designed to target the coding regions of either E6 and E7. The three HPV-positive cell lines were transfected with these siRNA sequences (189, 586 and 497), and silencing of both E6 and E7 genes was achieved by all sequences targeting different regions of the single bicistronic pre-mRNA of E6 and E7 (Supporting Information Fig. S1)Cells were treated with 10nM siRNA for 48h, after which mRNA expression was analyzed by RT-PCR. Sequence 189 (siE6) exhibited high silencing potency, with ~85% knockdown of E6 and E7 mRNA levels in 2A3 and UMSCC-104 cells compared to scrambled control siRNA (siNC), while the other siRNA sequences achieved lower reduction in target genes expression (Fig. 1B and Supporting Information Fig. S1).

Suppressed E6 and E7 mRNA levels induced by siE6 treatment had detrimental effect on the viability of HPV-positive cells. We observed extensive cell death by microscopic visualization of siE6-treated cultured cells (representative images in Supporting Information Fig. S1). We applied XTT assay to quantify cell death rates and found that the target genes knockdown translated into 40-60% reduction in viability of HPV-positive cells 72h after treatment. In contrast, none of the siRNA sequences inhibited the proliferation of the HPV-negative cell line, FaDu (Fig. 1C). We noted a greater reduction in E6/E7 expression and

more robust cell death in rapidly dividing cell lines (2A3 and UMSCC-104) compared to UPCI:SCC090 cells that have longer doubling time, typically >96h. These observations may clinically imply higher sensitivity of more aggressive and rapidly growing tumors to siE6 treatment. Immunoblotting revealed that suppression of E6/E7 by siE6 had led to upregulation of p53 in the HPV-positive cell lines but not the HPV-negative one, compared to siNC treatment (Fig. 1D). As demonstrated in Fig. 1D, treatment with siE6 resulted in a 19-, 44- and 4.6-fold increase in p53 protein levels in 2A3, UMSCC-104 and UPCI:SCC090, respectively, compared to siNC-treated cells. Interestingly, although we found a ~100-fold lower baseline mRNA and protein expression of E6 and E7 in 2A3 cells, compared to cell lines derived from patients initially infected with HPV-16 (Fig. 1A), p53 protein levels were markedly supressed in 2A3 cells and restored by siE6 treatment. This finding emphasizes the potent inhibition of p53 by HPV-E6, even with relatively low expression. Overall, our results validated the expected p53 protein recovery by anti-HPV-E6/E7 siRNA treatment and diminished proliferation of HPV-positive HNC cells induced by E6 and E7 knockdown *in vitro*.

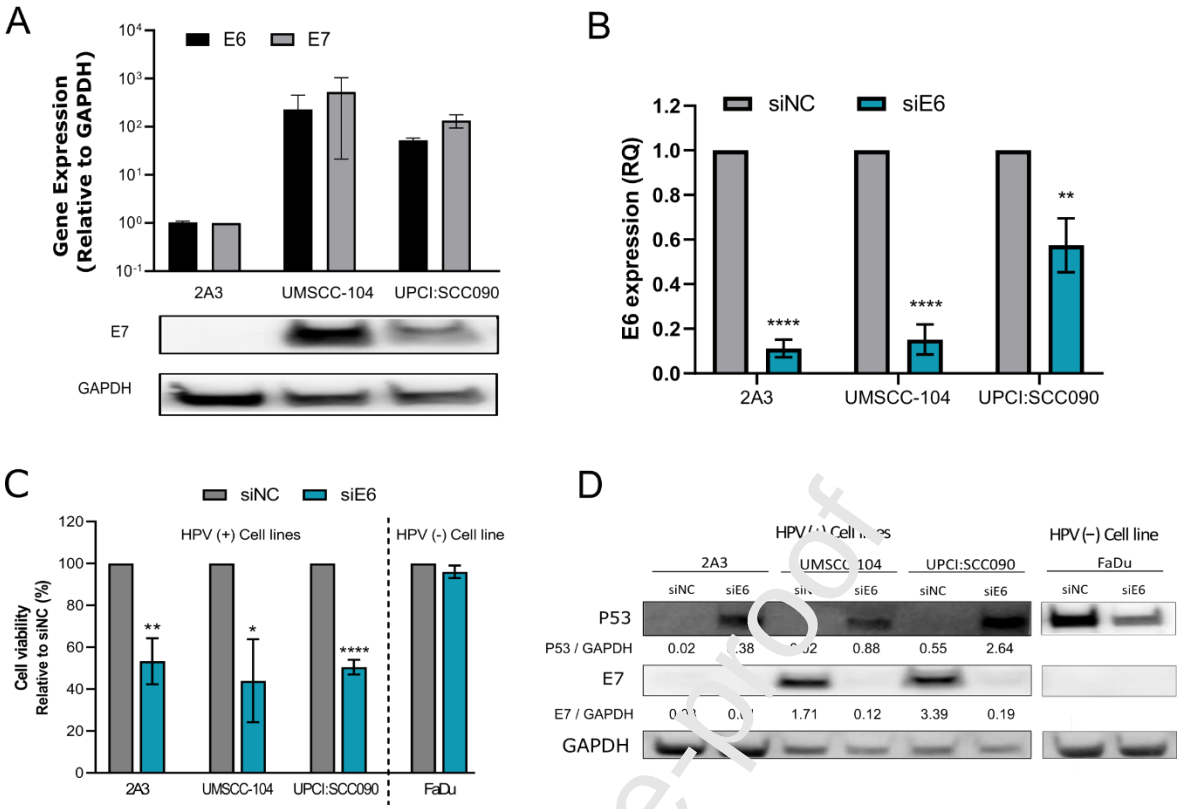

Fig. 1. HPV E6/E7 silencing suppresses cell proliferation and restores p53 in HPV-positive HNC cells. **A**, Detection of HPV E6/E7 in HPV16-positive HNC cell lines: 2A3, UMSCC-104 and UPCI:SCC090 by RT-PCR and western blot analysis. **B**, Target gene expression in three HPV positive cell lines 48h after siE6 treatment compared to scrambled control siRNA (siNC), measured by RT-PCR. Data are representative of three independent experiments, two-tailed Student's t-test, **, p<0.005, ****, p<0.00005. **C**, Viability 72h after siE6 treatment compared to siNC. Results are mean ± SD from three six-plicates experiments, two-tailed Student's t-test, *, p<0.05, **, p<0.005, ****, p<0.00005. **D**, Immunoblotting for E7 and p53 72h after treatment with siE6 or siNC. GAPDH was used as a loading control. Numbers indicate p53/GAPDH and E7/GAPDH ratios, as determined by densitometric analysis.

3.2 *EGFR internalization upon antibody binding*

Selective delivery of LNPs into tumor cells relies on the engagement of a surface target which is exclusively or highly expressed on tumor cells and not on normal cells. High antigen availability for binding increases the accessibility of the therapeutic cargo at target site.[35] Utilizing an internalizing ligand for targeting facilitates uptake by target cells and

intracellular trafficking of the LNPs. Rapid receptor-mediated endocytosis and recycling enables even more efficient release of cargo inside the cell.[36,37] Among the various potential surface targets, EGFR was reported to initiate rapid endocytosis, and thereby to constitute an effective targetable receptor.[37]

To verify EGFR overexpression on HPV-positive HNC cells and receptor-mediated internalization, cells were incubated with anti-human EGFR mAbs and analyzed by flow cytometry. We first allowed anti-EGFR mAbs to bind the cells at 4 ^{O}C. Unbound antibodies were washed out, after which cells were either kept on ice or incubated at 37 ^{O}C, to allow for receptor-mediated internalization to occur. Alexa-Fluor (AF) 647-labelled secondary antibodies were then added, and fluorescence intensity was read by the flow cytometer. We found high baseline EGFR density on FaDu, 2A3, UPCI:SCC090 and UMSCC-104 cells and observed dropping AF647 fluorescence intensity as incubation with primary anti-EGFR antibody was extended, providing evidence for EGFR-mediated internalization (Fig. 2A and Supporting Information Fig. S2). Contrarily, other members of the Erb family, such as HER2 and HER3, were not overexpressed on the surface of HNC cells and did not demonstrate similar patterns of internalization upon antibody binding (Supporting Information Fig. 2S). This set of experiments demonstrated that EGFR can serve as a targetable surface marker and indicated EGFR potential utility for intracellular delivery of LNPs.

3.3 *The ultra-structure of targeted LNPs*

LNPs entrapping siRNA were constructed with the NanoAssembler microfluidic mixing system as previously described.[33] The combining of acidified siRNAs (pH 4) with a mixture of lipids (cholesterol, DSPC, PEG-DMG, EA-PIP, and DSPE-PEG-Ome) resulted in the production of LNPs highly uniform in size with a mean diameter of 67nm as measured by

dynamic light scattering (DLS), and a minimally negative charge at physiological pH (Table 1). Targeting was attained by applying ASSET (Anchored Secondary scFv Enabling Targeting) linker strategy for mAbs conjugation,[30] which is based on a recombinant protein linker that enables uniform antibody attachment in a non-covalent method. Fig. 2B is a schematic diagram of the production process of tLNPs using the ASSET strategy. ASSET-LNPs conjugates were coated with either anti-human EGFR mAbs (tLNPs) or isotype antibodies (iso-LNPs). An ASSET:antibody ratio of ~1:1 forms highly stable constructs with 100% bio-conjugation as previously reported.[30] Moreover, while chemically conjugated antibodies are randomly oriented, the ASSET binds the Fc domain of the antibody, keeping the variable domain exposed for ligand binding (Fig. 2B). This design keeps the antibodies anchored to the LNPs functional, and allows high affinity binding of the targeted LNPs to the target ligand/receptor. ASSET- antibody conjugate slightly increased the LNPs mean diameter and size distribution, while the ζ-potential remained slightly negative (Table 1). Transmission electron microscopy images showed spherically shaped LNPs, validating their uniformity (Fig. 2C). Functionality of the targeting strategy was evaluated with Cy5-labelled siRNA entrapped in the LNPs. Higher fluorescence intensity measured from cells incubated with tLNPs at 4 ^{O}C verified more efficient binding compared to that of iso-LNPs (Fig. 2D). Internalization of tLNPs and iso-LNPs encapsulating Cy5-labelled siRNA was studied and visualized by confocal microscopy (Supporting information S3). Overall, utilizing ASSET technology for targeting mediated efficient target-cell binding without impeding the size or ultrastructure of the LNPs.

Table 1. Characterization of LNPs by Dynamic Light Scattering and ζ-Potential Measurements.

	uncoated LNPs	iso-LNPs	tLNPs
Hydrodynamic diameter [d,nm]	67 ± 6.4	95 ± 6.3	89 ± 7.6
Polydispersity index	0.11 ± 0.05	0.18 ± 0.09	0.13 ± 0.07
Z-potential [mV]	-3.02 ± 0.64	-3.50 ± 0.33	-5.04 ± 0.71

Data represent mean ± SD of six independent preparations

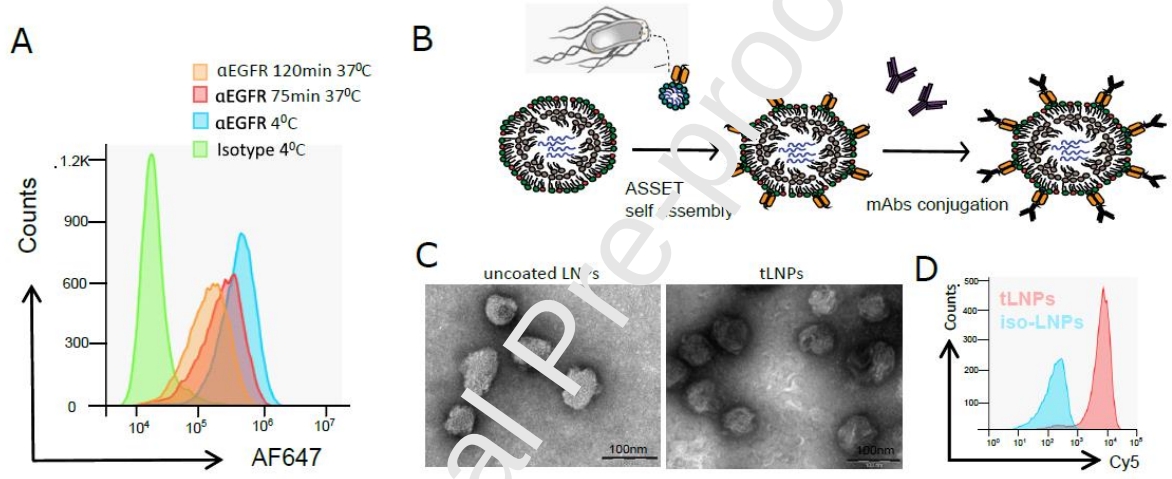

Fig. 2. EGFR coating mediates tLNPs binding to HNC cells without impeding ultra-structure of the LNPs. **A**, Anti-EGFR antibodies (AF647) binding (at 4 °C) and internalizing into UMSCC-104 cells when incubated at 37 °C. **B,** Schematic diagram of the production process of siRNA-loaded tLNPs using ASSET technology. ASSET, expressed in the E. coli periplasm anchored by lipidation to the inner membrane, is purified in micelles and inserted into the LNPs which are then coated with mAbs. Adopted with permission from Veiga *et al*, *Adv Drug Deliv Rev* 2020.[38] **C**, Representative transmission electron microscopy (TEM) images of uncoated LNPs (left) and tLNPs (right), 100nm scale bar. **D**, Binding to UMSCC-104 cells of tLNPs (red) or iso-LNPs (blue) encapsulating Cy5-labelled siRNA.

3.4 *Enhanced therapeutic effect of targeted LNPs in vitro*

The therapeutic efficacy of the tLNPs encapsulating the therapeutic siE6 in comparison to iso-LNPs and siContorl payload was initially tested *in vitro*. Cells were treated with the different LNPs-siRNA at a dose of 0.1μM, and alternations in protein expression and cell viability were evaluated 48, 72 and 96h after treatment. Down-regulation of E6 and E7 oncogenes is known to result in the liberation of p53 and Rb as cell cycle regulators which, in turn, leads to apoptotic cell death.[5,9] We found high silencing efficiency induced by tLNPs-siE6 treatment, as demonstrated by depressed levels of E6 mRNA and markedly reduced expression of E7 protein at 48h and 72h after treatment (Fig. 3A, Fig. 3B and Fig. 3C). Immunofluorescent staining showed the expected upregulation of cytoplasmic Rb along with diminished E7 protein levels (Fig. 3A). Interestingly, treatment with tLNPs encapsulating siNC also led to somewhat reduced E6 and E7 levels, reflected by large standard deviation of tLNPs-siNC bar, suggesting variable E6 mRNA expression levels (Fig. 3B). It also resulted in reduced expression of E7 protein (by 15%) compared to iso-LNPs-siNC treatment, observed in the immunoblotting panel (Fig. 3C). These findings are in accordance with previous reports suggesting that EGF signalling determines E6/E7 mRNA expression. [39,40] Depletion of EGF was shown to modulate splicing of the polycistronic E6/E7 mRNA, towards the exclusion of a certain fragment in the E6 open-reading frame (ORF), leading to a frameshift and a premature termination codon, producing the E6*protein.[39] The E6* protein was shown to counteract the E6 protein, thereby rescuing p53.[41] Therefore, it is reasonable to assume that the reduction in HPV oncogenes expression observed in tLNPs-siNC treated cells compared to iso-LNPs-siNC treated cells (Figure 3B and 3C) had been induced by the anti-EGFR mAbs. This effect can contribute to the therapeutic efficacy of tLNPs-siE6 in HPV-positive cells.

Another therapeutic advantage of tLNPs over iso-LNPs was revealed by flow cytometry analysis of Annexin V/PI staining 96h after LNPs treatment (Fig. 3D). The

tLNPs-siE6 exhibited greater induction of apoptosis compared to uncoated LNPs-siE6 or iso-LNPs-siE6 (apoptotic cells: 31.4% *vs*. 18.5% and 17.46%, respectively, $p<0.005$, two-way ANOVA). In addition, treatment with tLNPs, regardless of the siRNA cargo, resulted in significantly higher rates of apoptotic cell death compared to uncoated or iso-LNPs. Treatment of HPV-negative cells (FaDu) with tLNPs also resulted in slightly higher apoptotic cell death compared to iso-LNPs, but the difference was insignificant and less noticeable than the effect of tLNPs on HPV-positive cells. A possible explanation for the enhanced induction of apoptosis in HPV-positive cells could derive from the essential role of EGFR signalling pathways in cell proliferation, survival and differentiation. [27] EGFR signalling has been suggested to be particularly pivotal for the transforming activity of HPV16 E6/E7. [42] It has been suggested that EGFR stimulation in HPV-infected cells increases genetic instability, deregulation of proliferation and resistance to apoptosis by the activation of the PI3K/Akt/mTOR signalling pathway.[43] Several *in vitro* models have demonstrated that HPV E6/E7 directly stimulate Akt by its phosphorylation[44] which, in turn, amplify PI3K activation and generate resistance to anoikis and blockade of p53-induced cell death.[45] Activated Akt also interacts with E2F1 to depress its proapoptotic activity.[46] HPV E7 can further inhibit dephosphorylation of phosphorylated Akt, leading to constitutive Akt activation. HPV-positive cells were found to be more sensitive to EGFR inhibition compared to HPV-negative cells, demonstrated by inhibited clonal growth, stimulated apoptosis and pre-mature senescence of the former.[40,42] For example, lapatinib, a dual EGFR and HER2 inhibitor, was shown to specifically reduce Akt phosphorylation solely in HPV-positive cell lines with reduced expression of E6 and E7.[40] Consistent with these data, our findings also indicate that the tLNPs which incorporate anti-EGFR mAbs induced greater growth inhibition in HPV-positive cells compared to HPV-negative cells.

Taken together, the present results demonstrate that the tLNPs-siE6 successfully manipulated E6/E7 gene expression and subsequently induced marked apoptotic cell death of HPV-positive cells. We showed that the tLNPs outperformed uncoated or iso-LNPs in the induction of cell death, having observed significant rates of apoptosis after treatment with tLNPs. This finding could be attributed to direct anti-tumor activity of the anti-EGFR mAbs in HPV-positive cells, or to the translational regulation of functionally distinct E6 and E7 proteins induced by EGF signalling. We therefore conclude that the anti-EGFR mAbs constitute excellent targeting moieties that not only mediate intracellular delivery of encapsulated cargo, but also potentiate the therapeutic effect of siE6 in HPV-positive cells.

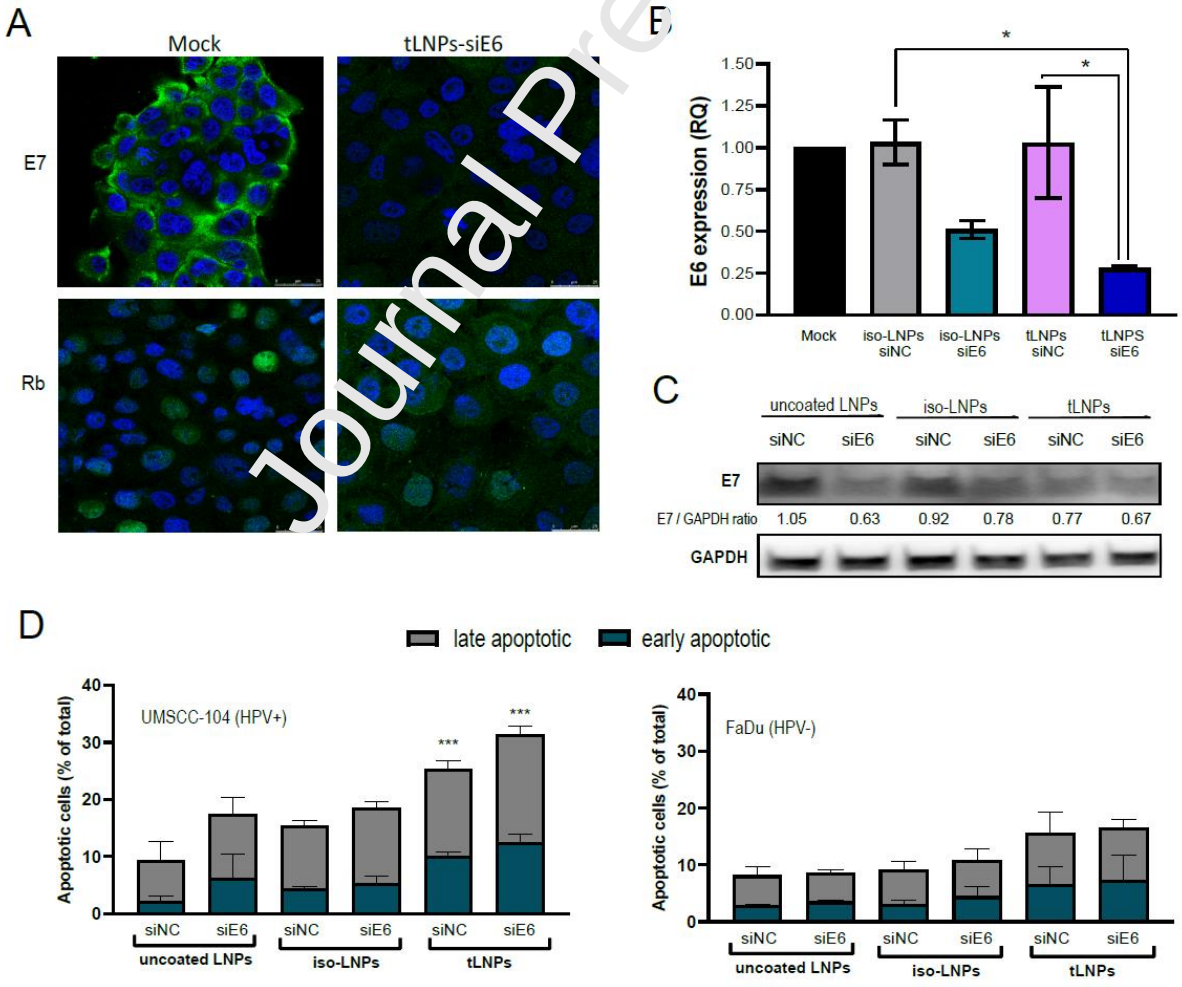

Fig. 3. tLNPs-siE6 suppress E6 and E7 expression and lead to apoptotic cell death of HPV-positive HNSCC cells. **A**, Confocal images of untreated UMSCC-104 cells (Mock) or tLNPs-siE6-treated cells, stained for E7 (top, green) and Rb (bottom, green) 72h after treatment. Nuclei were stained with DAPI (blue). **B**, Relative E6 expression in UMSCC-104 cells 48h after different LNPs-siRNA treatments, as measured by RT-PCR. Data represent the mean±SD of three independent experiments, one-way ANOVA, *p<0.05. **C,** Immunoblotting for E7 72h after treatment. GAPDH served as a loading control. **D**, Annexin V/PI staining of UMSCC-104 and FaDu cells 96h after treatment with siNC or siE6 encapsulated in uncoated, iso- or tLNPs. Results are mean ±SD of three independent experiments, 2-way ANOVA, *** p<0.0005.

3.5 *Uptake of tLNPs by tumor cells in vivo*

A xenograft HNC mouse model was established in order to determine whether EGFR-directed targeting improves systemic LNPs delivery and uptake in tumor cells. UMSCC-104 cells were inoculated subcutaneously in the flanks of 8-week-old female FoxN1 nude mice. Once the tumors had reached approximately 100 mm^3, the mice were intravenously (iv) injected with either tLNPs or iso-LNPs encapsulating Cy5-labelled siRNA (1mg siRNA/kg body weight). The pharmaco-kinetic profile was assessed by quantifying Cy5 fluorescence intensity in plasma samples drawn at 0.25, 0.5, 1 and 2h after LNPs iv administration. We observed rapid clearance of Cy5-labelled LNPs from circulation (Supporting Information Fig. S4). Whole body imaging by an IVIS imaging system of tumor-bearing mice injected with iso-LNPs or tLNPs at 2h post-injection revealed visible localization of both iso-LNPs and tLNPs at the tumor site (representative images, Fig. 4A).

We further evaluated the biodistribution to normal tissues *versus* the xenograft tumors utilizing the Cy5-labeled LNPs. Iso-LNPs and tLNPs were iv injected to tumor-bearing mice, and organs and tumors were harvested and analyzed 4h and 24h post-injection. We observed comparable distribution to healthy tissues at 4h and 24h after iv injection of iso-LNPs and tLNPs, with high LNPs accumulation in the liver and spleen (Fig. 4B, Fig. 4C and Supporting

Information Fig. S4). Both iso-LNPs and t-LNPs reached the tumor xenografts at 4h and 24h post-injection, but the mean average radiance of the Cy5 signal in the xenograft tumors was ~10-fold and ~100-fold lower than in the liver at 4h and 24h post- injection, respectively (Fig. 4B and Fig. 4C). We noted higher Cy5 fluorescence intensity in the tumors of tLNPs-injected mice compared to tumors of the iso-LNPs-injected mice, but these differences did not reach statistical significance (Fig. 4D and Fig. 4E, p>0.05, two-tailed unpaired Student's t-test).

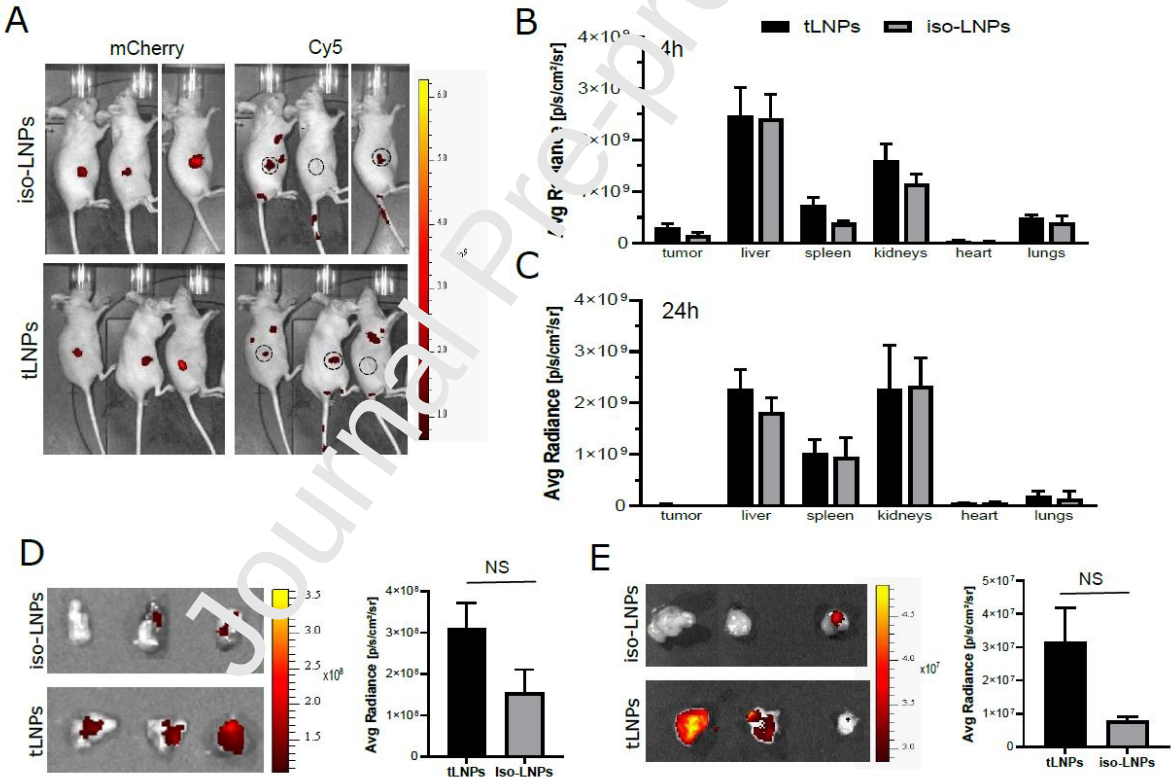

Fig. 4. Biodistribution and tumor accumulation of tLNPs and iso-LNPs in xenograft tumor-bearing mice. **A**, Representative IVIS images of mCherry signal (tumor cells) and Cy5 signal (LNPs) in tumor bearing mice 2h post-injection with either iso-LNPs or tLNPs. In the images of Cy5 fluorescence the tumors are marked by dashed circles. **B-C,** Biodistribution of Cy5-labelled iso-LNPs and tLNPs at 4h (B) and 24h (C) post-injection (n=6 mice per group). **D-E**, Representative IVIS images of the tumors harvested from mice at 4h (D) and 24h (E) after iv LNPs administration, and quantification of Cy5 fluorescence intensity by living image software comparing iso-LNPs *vs*.

tLNPs tumor uptake (n=6 mice per time point). NS, not significant. Data (**B-E**) are representative of two independent experiments per time point (4h and 24h).

Cy5-labelled LNPs were employed to further investigate tumor localization and tLNPs uptake selectively by tumor cells. Tumor-bearing mice were iv injected with iso-LNPs or tLNPs, and the tumors were harvested 4h later. Cryosections were performed to determine the intra-tumoral distribution of the LNPs. In accordance with the IVIS imaging findings, both iso-LNPs and tLNPs were widely distributed throughout the tumors, indicating comparable successful extravasation through tumor vessels. However, high-power magnification revealed distinctive patterns of intra-tumoral distribution for tLNPs compared to iso-LNPs. We observed that tLNPs were localized in direct association with cell surface of tumor cells, stained by anti-human EGFR antibodies, or within the tumor cells (Fig. 5, white arrows). On the contrary, iso-LNPs were predominantly distributed in tumoral interstitial matrix where anti-human EGFR-labelling was absent (orange arrows). Iso-LNPs were mostly found in areas where smaller nuclei cells reside and where the lack of EGFR surface marking was prominent. Based on these observations, we suggest that utilizing the anti-EGFR mAbs improve local retention of tLNPs and selective uptake by the target cells.

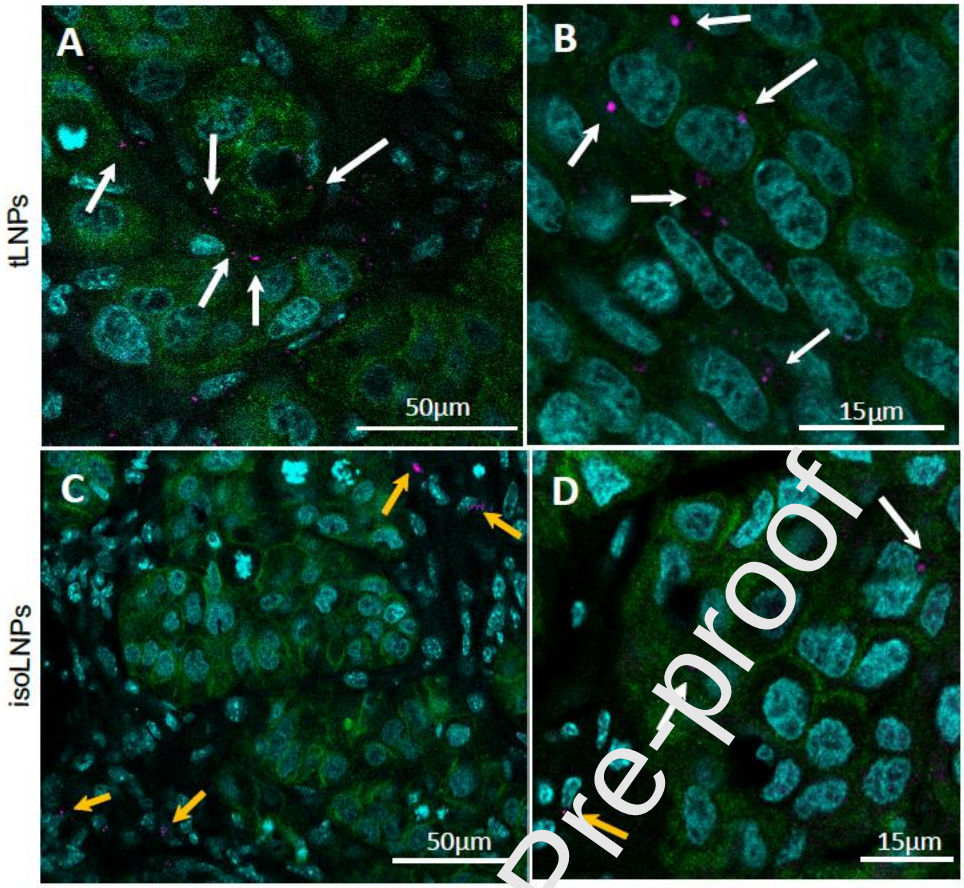

Fig. 5. Active targeting enhances LNPs uptake by tumor cells. Tumors were excised 4h post injection of iso-LNPs or tLNPs, and cryosections stained for EGFR (green), to mark tumor cell surface, and DAPI (blue) to label nuclei. LNPs were visualized by Cy5 fluorescence (magenta). **A-B** tLNPs were found in close association with the surface of tumor cells or taken up by tumor cells (white arrows). In contrast, iso-LNPs were mostly in the interstitial matrix (orange arrows) as identified by dense areas of smaller-nuclei cells compared to tumor cells (C-D). Images are representative of two independent experiments.

3.6 *tLNPs-siE6 impede xenograft tumor growth in vivo*

We used a xenograft mice model to test the efficacy of tLNPs encapsulating siE6. UMSCC-104 cells were inoculated subcutaneously in the mice flanks, and tumor growth was

monitored twice weekly. When the tumors had reached a volume of approximately 50mm^3 (12 days after cell inoculation), the mice were iv injected with tLNPs-siE6, iso-LNPs-siE6, tLNPs-siNC or iso-LNPs-siNC (1mg siRNA/kg body weight). A total of 6 doses were administered, at 3- to 4- day intervals. Treatment response was monitored by consecutive tumor volume measurements (Fig. 6A and Supporting information Fig. S5). We found significant restriction of tumor growth in the mice treated with tLNPs encapsulating siE6 compared to the mice that were treated with iso-LNPs-siNC ($p<0.05$ on days 21, 25 and 31, Fig. 6A). We also noticed that treatment with tLNPs encapsulating siNC slowed tumor growth rate, indicating anti-tumor activity mediated solely by the targeting moieties. This observation provides *in vivo* evidence for the therapeutic advantage of utilizing the anti-EGFR mAbs for targeting, and supports our claim that the targeting antibodies are not inert.

Decrease in E6 and E7 mRNA levels was observed in tumors extracted from mice treated with either tLNPs-siE6 or iso-LNPs-siE6 (Fig. 6B). Reduction in E7 expression was also evident in tumors of mice injected with tLNPS-siNC. This finding is in agreement with our *in vitro* findings (Fig. 3) both implying that EGFR signalling determined E6/E7 bicistronic mRNA splicing, as also suggested by others.[39]

H&E staining showed scant areas of viable cells in siE6-treated tumors compared to control treatments. Immunohistochemical (IHC) detection of P16 is widely used as a surrogate marker for HPV infection, and commonly replaces HPV-specific tests in the clinical setup due to lower costs. P16 acts as a tumor suppressor. When HPV E7 binds Rb, it effectively stops Rb negative feedback on P16. Less intense P16 staining observed by IHC indicates down-regulation of HPV in siE6-treated tumors (Fig. 6C). To confirm the mechanism of tumor growth inhibition and ascertain apoptosis induction, TUNEL assay was applied. Confocal images demonstrated more extensive TUNEL staining in the tumors extracted from mice treated with tLNP-siE6 compared to control groups (Fig. 6D).

The off-target toxicity of the LNPs-siRNA complexes was assessed by microscopic examination of several organs, that exhibited significant LNPs uptake in the biodistribution experiments. Organs were collected 72h after the last LNPs dose and prepared for histologic analysis. We found no abnormal morphology in the livers, spleens, hearts, lungs and kidneys after LNPs treatments, indicating the safety of the lipidic nanocarrier and its contents (Supporting Information Fig. S6).

Altogether, we were able to show therapeutic efficacy of tLNPs encapsulating siE6 *in vivo* by demonstrating tumor growth restriction, marked *in vivo* target genes knockdown, and positive TUNEL staining that confirmed apoptotic cell death.

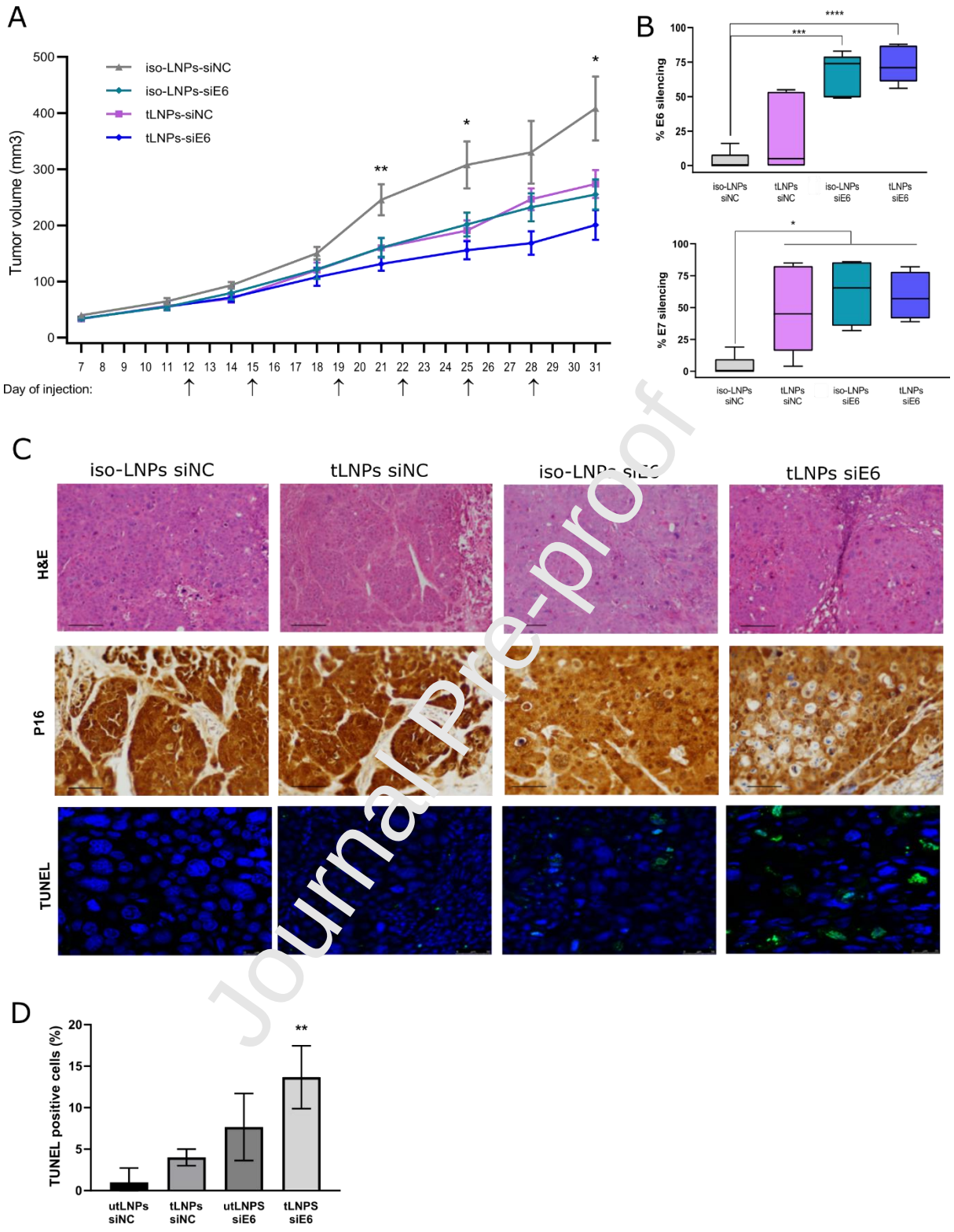

Fig. 6. αEGFR tLNP-siE6 mediates therapeutic gene silencing in a xenograft HPV-positive HNC mouse model. **A,** UMSCC-104 cells were subcutaneously inoculated in FoxN1 nude mice. After tumors had reached approximately 50 mm^3, mice were intravenously injected with tLNPs or iso-LNPs encapsulating siE6 or siNC on days 12,15,19,22,25 and 28, n=10 mice/group. Data are presented as mean ± SEM; one-way ANOVA, * p<0.05, ** p<0.005 tLNPs-siE6 *vs*. iso-LNPs-siNC **B**, *in vivo*

E6/E7 silencing in xenograft tumors by either tLNPs or iso-LNPs encapsulating siE6 or siNC, n=5 mice/group. Data are presented as interquartile range (IQR) with a median center line and minimum to maximum error bars; one-way ANOVA, * p<0.05, ***p<0.0005, ****p<0.00005 **C,** H&E staining (scale bar, 200μm), immunohistochemical staining of P16 (scale bar, 100 μm) and TUNEL staining of tumor tissues. **D**, Statistical analysis (mean ± SD) of the percentage of apoptotic cells in tumor tissues as determined by TUNEL assay (representative images in panel D). A total of 3 fields from each treatment group were counted. One-way ANOVA, ** p<0.005. Data (**A**-**D**) are representative of two independent experiments.

4. Discussion

The recent increase in the incidence of HNC in western world has been attributed to the upsurge of high-risk HPV infections.[2,3] There are still no specific therapies addressing the distinctive molecular mechanisms of HPV-induced transformation. The application of siRNA against HPV-E6 and E7 carries great potential for HPV-positive cancer treatment. However, its clinical translation, as for various other diseases, has been hindered by obstacles stemming from systemic delivery barriers, such as high immunogenicity, unstable nature of siRNA molecules and rapid clearance from circulation. Together with limited intracellular uptake, systemic administration of naked RNAi-based therapeutics is inefficient and even potentially harmful.[47] Previous efforts to generate delivery vehicles for siRNA based on lipidic particles have demonstrated promising results in HPV-positive cervical cancer mouse models.[48–50] Wu. *et al* [49] were the first to demonstrate a 50% reduction in tumor size by utilizing polyethylene glycol (PEG)ylated lipid particles for iv administration of E6/E7-targeted siRNA for the treatment of cervical cancer. Successful *in vivo* systemic delivery of anti-HPV siRNA to treat HPV-positive head and neck cancer has never been previously reported.

In this study, we aimed to explore the efficacy of systemically administered anti-HPV siRNA encapsulated in targeted LNPs by means of our recently developed modular targeting platform, the ASSET.[30] The ASSET technology enables coating of LNPs with monoclonal antibodies as targeting moieties. The paradigm of antibody-based targeted nanoparticles for cancer therapy has demonstrated major progress, especially exemplified by the clinical success of numerous therapeutic antibodies and immunoconjugates for various clinical applications, including solid tumors.[51] Targeting antibodies are hypothesized to specifically bind and internalize into cancer cells, thereby increasing the intracellular concentration of the cytotoxic drug while minimizing non-specific side effects. However, highly efficient nanocarriers first have to arrive at the tumor site, a process which mainly depends upon mechanical and biological aspects of systemic transport. Our findings are in agreement with previous reports, suggesting that more than 90% of the injected dose ends up in normal tissues. This biodistribution profile highlight the misconception that targeting can improve delivery to the target tumor.[52] Indeed, most studies report that the presence of targeting moieties on nanoparticles may be irrelevant in determining biodistribution and in enhancing tumor accumulation since tumor localization is based upon blood circulation. [20,52,53] Some would claim that the main mechanism allowing for the accumulation of therapeutic agents at a tumor site is the enhanced permeability and retention (EPR) effect, also known as “passive delivery” into solid tumors.[54] The vessels formed in the cancerous tissue are fragile, leaky and sustain viscous blood flow, resulting in greater vasculature permeability and efficient accumulation of macromolecules. The absence of functional lymphatic drainage results in greater retention in the interstitial space. It is reasonable to assume that the relatively small diameter (<100nm) and nearly neutral zeta potential of both iso-LNPs and tLNPs were accountable for their comparably efficient extravasation and tumor deposition in the xenograft tumor model. Targeting did not result in preferential LNPs

accumulation in the tumor, compared to other organs, because it cannot facilitate the critical step of extravasation through tumor vessels.[53] It has been hypothesized, however, that active targeting increases nanocarrier retention at the target site by mediating greater binding to tumor cells which subsequently leads to improved drug delivery inside target cells.[23,24] In line with this hypothesis, an intra-tumoral distribution analysis following iso-LNPs and tLNPs injection to tumor-bearing mice confirmed that EGFR-directed targeting mediated greater LNPs arrival at tumor cells. We now demonstrated increased localization of tLNPs in tumor cells, while iso-LNPs were mostly distributed in the tumor stroma.

The targeting strategy we utilized has the important advantage of being simple and modular. The ASSET platform enables integration of a wide range of mAbs for targeting by a simple incubation with the LNPs that is potentially applicable to many other diseases. Moreover, targeting did not significantly change any physical properties of the LNPs, evidenced by their unaffected size and charge, according to the TEM and DLS measurements. Lastly, this targeting strategy enabled the generation of functional tLNPs, i.e, active antibodies that elicit anti tumor activity. Anti-EGFR monoclonal antibodies (e.g., cetuximab) are approved for clinical use in the indication of advanced stage HNC [28] and their role of replacing chemotherapeutic agents for HPV oropharyngeal cancer in order to reduce treatment toxicity is being under investigation. [55,56] In the current study, we showed greater tumor growth inhibition by treatment with tLNPs-siE6 compared to iso-LNPs-siNC. As tLNPs that encapsulate siNC also exhibited a certain inhibitory effect on tumor growth, their therapeutic effect can be attributed to the anchored antibodies. The amount of antibodies utilized for targeting LNPs and the amount applied for immunotherapy differ, thus precluding a comparison of the therapeutic efficacy of these modalities. However, we found that the targeting antibodies are not inert, and showed that they added to the

therapeutic effect of the delivered cargo. Specifically, in this model of HPV-positive HNC, the improved therapeutic effect of the tLNPs compared to iso-LNPs can be explained by several mechanisms: greater intracellular trafficking of the siRNA cargo through receptor-mediated endocytosis, modulation of the expression of HPV-oncogenes *via* alternative splicing regulated by EGFR activation, or simply by prevention of EGFR ligand binding, which inhibit receptor activation and downstream signalling.

HPV oncoproteins and EGFR, which are both targeted by the tLNPs-siE6 we have devised, are known to interact and promote tumorigenesis *via* common signalling pathways.[40,42,43] We hypothesized that synergistic or additive effect can be achieved by the siRNA cargo against HPV combined with functional anti-EGFR antibodies, acting simultaneously on different crucial targets in HPV-induced cancer. Though we could not demonstrate significantly higher inhibition of tumor growth by the combined approach (tLNPs-siE6) compared to that attained by each component separately (iso-LNPs-siE6 or tLNPs-siNC), our findings indicate that both the siRNA component and the targeting moiety act together to generate more efficient therapeutic outcome. Specifically, the *ex-vivo* microscopic analyses of tLNPs-siE6 treated tumors versus other therapies have clearly demonstrated more prominent positive TUNEL staining and lower intensity P16 staining as indicators of the desirable outcome. Certain modifications of the tLNPs-siE6 therapy, such as using more potent RNAi-based therapeutic cargo, or more intense treatment protocol may improve our findings. Further experiments are underway to reinforce the superiority of the combined strategy.

5. Conclusions

In this study, we have devised targeted LNPs that deliver anti-HPV-E6/E7 siRNA against HPV-induced HNC. We show that our targeting strategy, based on the ASSET linker technology to integrate antibodies to LNPs, has mediated precise delivery of tLNPs into target cells, indicated by greater tLNP binding to tumor cells *in vitro* and increased intracellular cargo delivery *in vivo* compared to iso-LNPs. In addition, we demonstrate that treatment with tLNPs, compared to iso-LNPs, has elicited greater anti-tumor effect, suggested by greater induction of apoptosis *in vitro* . Restriction of tumor growth *in vivo* was also observed however the superiority of the tLNPs-siE6 over other treatments was less prominent. Further studies are warranted. Ultimately, this treatment strategy may spare highly toxic chemo-radiotherapy from HPV-positive HNC patients by providing precise and specific inhibition of HPV. In a wider perspective, this combinational therapy using potent siRNA encapsulated in functional tLNPs can be further applied against various other diseases.

Data and material availability

All relevant data are available from the authors upon reasonable request.

Acknowledgments

This work was supported in part by grants from the ISF, EU Expert and Lewis Trust awarded to D.P, and by the Kahn Foundation grant awarded to L.K.

Credit Author Statement

Liyona Kampel: Conceptualization, methodology, investigation, data analysis and writing the original draft; **Meir Goldsmith**: Methodology, investigation and data analysis; **Srinivas Ramishetti;** Methodology, **Nuphar Veiga**: Methodology and data analysis ; **Daniel Rosenblum**: Methodology and data analysis; **Anna Gutkin**: Methodology and data analysis ; **Sushmita Chatterjee**: Methodology and data analysis, **Moran Penn**: Methodology and data analysis; **Galya Lerman**: Resources; **Dan Peer**: Conceptualization, supervision, reviewing and editing the final manuscript; **Nidal Muhanna**: Conceptualization, supervision, reviewing and editing the final manuscript

Conflict of interest

D.P. receives licensing fees (to patents on which he was an inventor) from, invested in, consults (or on scientific advisory boards or boards of directors) for, lectured (and received a fee) or conducts sponsored research at TAU for the following entities: Alnylam Pharmaceuticals Inc. Arix Biosciences Inc., ART Biosciences, BioNtech RNA pharmaceuticals; Centricus, Diagnostear Ltd., EPM Inc., Earli Inc., lmpetis Biosciences, Kernal Biologics, GPCR Inc., Medison Pharma Ltd., Newphase Ltd, NLC Pharma Ltd., Nanocell Therapeutics, NanoGhosts Ltd. , Precision Nanosystems Inc., Paul Hastings Inc., Regulon, Roche, SciCann, Shire Inc., VLX Ventures, TATA Cooperation, Teva Pharmaceuticals Inc., Wize Pharma Ltd. All other authors declare no competing financial interests.

Supplementary data

Supplementary material

References

[1] L.A. Torre, F. Bray, R.L. Siegel, J. Ferlay, J. Lortet-tieulent, A. Jemal, Global Cancer Statistics, 2012, CA a Cancer J. Clin. 65 (2015) 87–108. https://doi.org/10.3322/caac.21262.

[2] J. Mork, A.K. Lie, E. Glattre, S. Clark, G. Hallmans, E. Jellum, P. Koskela, B. Møller, E. Pukkala, J.T. Schiller, Z. Wang, L. Youngman, M. Lehtinen, J. Dillner, Human Papillomavirus Infection as a Risk Factor for Squamous-Cell Carcinoma of the Head and Neck, N. Engl. J. Med. 344 (2001) 1125–1131. https://doi.org/10.1056/NEJM200104123441503.

[3] K.B. Pytynia, K.R. Dahlstrom, E.M. Sturgis, Epidemiology of HPV-associated oropharyngeal cancer, Oral Oncol. 50 (2014) 380–386.

https://doi.org/10.1016/j.oraloncology.2013.12.019.

[4] A.K. Chaturvedi, E.A. Engels, R.M. Pfeiffer, B.Y. Hernandez, W. Xiao, E. Kim, B. Jiang, M.T. Goodman, M. Sibug-Saber, W. Cozen, L. Liu, C.F. Lynch, N. Wentzensen, R.C. Jordan, S. Altekruse, W.F. Anderson, P.S. Rosenberg, M.L. Gillison, Human papillomavirus and rising oropharyngeal cancer incidence in the United States, J. Clin. Oncol. 29 (2011) 4294–4301. https://doi.org/10.1200/JCO.2011.36.4596.

[5] D. Sano, N. Oridate, The molecular mechanism of human papillomavirus - induced carcinogenesis in head and neck squamous cell carcinoma., Int. J. Clin. Oncol. 21 (2016) 819–826. https://doi.org/10.1007/s10147-016-1005-x.

[6] K. Münger, A. Baldwin, K.M. Edwards, H. Hayakawa, C.L. Nguyen, M. Owens, M. Grace, K. Huh, Mechanisms of Human Papillomavirus-Induced Oncogenesis, J. Virol. (2004). https://doi.org/10.1128/jvi.78.21.11451-11460.2004.

[7] M. Scheffner, J.M. Huibregtse, The HPV-16 E6 and EG-AP Complex Functions as a Ubiquitin-Protein Ligase in the Ubiquitination of ~ 53, 75 (1993) 495–505.

[8] K. Butz, T. Ristriani, A. Hengstermann, C. Denk, M. Scheffner, F. Hoppe-Seyler, siRNA targeting of the viral E6 oncogene efficiently kills human papillomavirus-positive cancer cells, Oncogene. 22 (2003) 5938–5945. https://doi.org/10.1038/sj.onc.1206894.

[9] C. Li, D.E. Johnson, Liberation of functional p53 by proteasome inhibition in human papilloma virus positive head and neck squamous cell carcinoma cells promotes apoptosis and cell cycle arrest., Cell Cycle. 12 (2013) 923–34. https://doi.org/10.4161/cc.23882.

[10] T. Fujii, M. Saito, E. Iwasaki, T. Ochiya, Y. Takei, S. Hayashi, A. Ono, N. Hirao, M. Nakamura, K. Kubushiro, K. Tsukazaki, D. Aoki, Intratumor injection of small interfering RNA-targeting human papillomavirus 18 E6 and E7 successfully inhibits the growth of cervical cancer, Int. J. Oncol. (2006). https://doi.org/10.3892/ijo.29.3.541.

[11] Z. Adhim, N. Otsuki, J. Kitamoto, N. Morishita, M. Kawabata, T. Shirakawa, K.I. Nibu, Gene silencing with siRNA targeting E6/E7 as a therapeutic intervention against

head and neck cancer-containing HPV16 cell lines, Acta Otolaryngol. 133 (2013) 761–771. https://doi.org/10.3109/00016489.2013.773405.

[12] L.C. Gomes-Da-Silva, S. Simões, J.N. Moreira, Challenging the future of siRNA therapeutics against cancer: The crucial role of nanotechnology, Cell. Mol. Life Sci. (2014). https://doi.org/10.1007/s00018-013-1502-2.

[13] K. Tatiparti, S. Sau, S.K. Kashaw, A.K. Iyer, siRNA delivery strategies: A comprehensive review of recent developments, Nanomaterials. (2017). https://doi.org/10.3390/nano7040077.

[14] A. Daka, D. Peer, RNAi-based nanomedicines for targeted personalized therapy, Adv. Drug Deliv. Rev. (2012). https://doi.org/10.1016/j.addr.2012.08.014.

[15] D. Peer, J. Lieberman, Special delivery: Targeted therapy with small RNAs, Gene Ther. 18 (2011) 1127–1133. https://doi.org/10.1038/gt.2011.56.

[16] T.J. Anchordoquy, Y. Barenholz, D. Boraschi, M. Chorny, P. Decuzzi, M.A. Dobrovolskaia, Z.S. Farhangrazi, D. Farrell, A. Gabizon, H. Ghandehari, B. Godin, N.M. La-Beck, J. Ljubimova, S.M. Moghimi, L. Pagliaro, J.H. Park, D. Peer, E. Ruoslahti, N.J. Serkova, D. Simberg, Mechanisms and Barriers in Cancer Nanomedicine: Addressing Challenges, Looking for Solutions, ACS Nano. 11 (2017) 12–18. https://doi.org/10.1021/acsnano.6b08244.

[17] M.E. Davis, The First Targeted Delivery of siRNA in Humans via a Nanoparticle : From Concept to Clinic, Mol. Pharm. (2009). https://doi.org/10.1021/mp900015y.

[18] J. Tabernero, G.I. Shapiro, P.M. LoRusso, A. Cervantes, G.K. Schwartz, G.J. Weiss, L. Paz-Ares, D.C. Cho, J.R. Infante, M. Alsina, M.M. Gounder, R. Falzone, J. Harrop, A.C.S. White, I. Toudjarska, D. Bumcrot, R.E. Meyers, G. Hinkle, N. Svrzikapa, R.M. Hutabarat, V.A. Clausen, J. Cehelsky, S. V. Nochur, C. Gamba-Vitalo, A.K. Vaishnaw, D.W.Y. Sah, J.A. Gollob, H.A. Burris, First-in-humans trial of an RNA interference therapeutic targeting VEGF and KSP in cancer patients with liver involvement, Cancer Discov. (2013). https://doi.org/10.1158/2159-8290.CD-12-0429.

[19] B. Schultheis, D. Strumberg, A. Santel, C. Vank, F. Gebhardt, O. Keil, C. Lange, K. Giese, J. Kaufmann, M. Khan, J. Drevs, First-in-human phase I study of the liposomal RNA interference therapeutic Atu027 in patients with advanced solid tumors, J. Clin.

Oncol. (2014). https://doi.org/10.1200/JCO.2013.55.0376.

[20] R.K. Jain, T. Stylianopoulos, Delivering nanomedicine to solid tumors, Nat. Rev. Clin. Oncol. (2010). https://doi.org/10.1038/nrclinonc.2010.139.

[21] H.J. Kim, Y. Yi, A. Kim, K. Miyata, Small Delivery Vehicles of siRNA for Enhanced Cancer Targeting, Biomacromolecules. 19 (2018) 2377–2390. https://doi.org/10.1021/acs.biomac.8b00546.

[22] S. Wilhelm, A.J. Tavares, Q. Dai, S. Ohta, J. Audet, H.F. Dvorak, W.C.W. Chan, Analysis of nanoparticle delivery to tumours, Nat. Rev. Mater. 1 (2016). https://doi.org/10.1038/natrevmats.2016.14.

[23] J. Shi, Z. Xiao, N. Kamaly, O.C. Farokhzad, Self-assembled targeted nanoparticles: Evolution of technologies and bench to bedside translation, Acc. Chem. Res. (2011). https://doi.org/10.1021/ar200054n.

[24] N. Bertrand, J. Wu, X. Xu, N. Kamaly, O.C. Farokhzad, Cancer nanotechnology: The impact of passive and active targeting in the era of modern cancer biology, Adv. Drug Deliv. Rev. (2014). https://doi.org/10.1016/j.addr.2013.11.009.

[25] D. Rosenblum, N. Joshi, W. Tao, J.M. Karp, D. Peer, Progress and challenges towards targeted delivery of cancer therapeutics, Nat. Commun. 9 (2018). https://doi.org/10.1038/s41467-018-03705-y.

[26] J.R. Grandis, D.J. Tweardy, Elevated Levels of Transforming Growth Factor a and Epidermal Growth Factor Receptor Messenger RNA Are Early Markers of Carcinogenesis in Head and Neck Cancer1, (1993) 3579–3585.

[27] S. Sigismund, D. Avanzato, L. Lanzetti, Emerging functions of the EGFR in cancer, Mol. Oncol. (2018). https://doi.org/10.1002/1878-0261.12155.

[28] J.B. Vermorken, J. Trigo, R. Hitt, P. Koralewski, E. Diaz-Rubio, F. Rolland, R. Knecht, N. Amellal, A. Schueler, J. Baselga, Open-label, uncontrolled, multicenter phase II study to evaluate the efficacy and toxicity of cetuximab as a single agent in patients with recurrent and/or metastatic squamous cell carcinoma of the head and neck who failed to respond to platinum-based the, J. Clin. Oncol. 25 (2007) 2171–2177. https://doi.org/10.1200/JCO.2006.06.7447.

[29] M.S. Kies, F.C. Holsinger, J.J. Lee, W.N. William, B.S. Glisson, H.Y. Lin, J.S. Lewin,

L.E. Ginsberg, K.A. Gillaspy, E. Massarelli, L. Byers, S.M. Lippman, W.K. Hong, A.K. El-Naggar, A.S. Garden, V. Papadimitrakopoulou, Induction chemotherapy and cetuximab for locally advanced squamous cell carcinoma of the head and neck: Results from a phase II prospective trial, J. Clin. Oncol. 28 (2010) 8–14. https://doi.org/10.1200/JCO.2009.23.0425.

[30] R. Kedmi, N. Veiga, S. Ramishetti, M. Goldsmith, D. Rosenblum, N. Dammes, I. Hazan-Halevy, L. Nahary, S. Leviatan-Ben-Arye, M. Harlev, M. Behlke, I. Benhar, J. Lieberman, D. Peer, A modular platform for targeted RNAi therapeutics, Nat. Nanotechnol. 13 (2018) 214–219. https://doi.org/10.1038/s41565-017-0043-5.

[31] K. Yamato, T. Yamada, M. Kizaki, K. Ui-Tei, Y. Natori, M. Fujino, T. Nishihara, Y. Ikeda, Y. Nasu, K. Saigo, M. Yoshinouchi, New highly potent and specific E6 and E7 siRNAs for treatment of HPV16 positive cervical cancer, Cancer Gene Ther. 15 (2008) 140–153. https://doi.org/10.1038/sj.cgt.7701113.

[32] S. Ramishetti, I. Hazan-Halevy, R. Palakuri, S. Chatterjee, S. Naidu Gonna, N. Dammes, I. Freilich, L. Kolik Shmuel, D. Danino, D. Peer, A Combinatorial Library of Lipid Nanoparticles for RNA Delivery to Leukocytes, Adv. Mater. 32 (2020) 1–8. https://doi.org/10.1002/adma.201906128.

[33] S. Ramishetti, R. Kedmi, M. Goldsmith, F. Leonard, A.G. Sprague, B. Godin, M. Gozin, P.R. Cullis, D.M. Dykxhoorn, D. Peer, Systemic Gene Silencing in Primary T Lymphocytes Using Targeted Lipid Nanoparticles, (2015) 6706–6716.

[34] S. Tang, M. Tao, J.P.M. Jr, J.P. Mccoy, Z. Zheng, The E7 Oncoprotein Is Translated from Spliced E6 * I Transcripts in High-Risk Human Papillomavirus Type 16- or Type 18-Positive Cervical Cancer Cell Lines via Translation Reinitiation The E7 Oncoprotein Is Translated from Spliced E6 * I Transcripts in Hig, J. Virol. 80 (2006) 4249–4263. https://doi.org/10.1128/JVI.80.9.4249.

[35] S.H. Alavizadeh, F. Soltani, M. Ramezani, Recent Advances in Immunoliposome-Based Cancer Therapy, Curr. Pharmacol. Reports. (2016). https://doi.org/10.1007/s40495-016-0056-z.

[36] C.M. Varga, T.J. Wickham, D.A. Lauffenburger, Receptor-mediated targeting of gene delivery vectors: Insights from molecular mechanisms for improved vehicle design, Biotechnol. Bioeng. (2000). https://doi.org/10.1002/1097-

0290(20001220)70:6<593::AID-BIT1>3.0.CO;2-N.

[37] T. Tashima, Effective cancer therapy based on selective drug delivery into cells across their membrane using receptor-mediated endocytosis, Bioorganic Med. Chem. Lett. (2018). https://doi.org/10.1016/j.bmcl.2018.07.012.

[38] N. Veiga, Y. Diesendruck, D. Peer, Targeted lipid nanoparticles for RNA therapeutics and immunomodulation in leukocytes, Adv. Drug Deliv. Rev. (2020). https://doi.org/10.1016/j.addr.2020.04.002.

[39] S. Rosenberger, J.D. Arce, L. Langbein, R.D.M. Steenbergen, F. Rösl, Alternative splicing of human papillomavirus type-16 E6 / E6 * early mRNA is coupled to EGF signaling via, 107 (2010) 7006–7011. https://doi.org/10.1073/pnas.1002620107.

[40] I. Fumagalli, D. Dugue, J.E. Bibault, C. Clémenson, M.C. Vozenin, M. Mondini, E. Deutsch, Cytotoxic effect of lapatinib is restricted to human papillomavirus-positive head and neck squamous cell carcinoma cell lines, Onco. Targets. Ther. 8 (2015) 335–345. https://doi.org/10.2147/OTT.S68225.

[41] D. Pim, L. Banks, HPV-18 E6*I protein modulates the E6-directed degradation of p53 by binding to full-length HPV-18 E6, Oncogene. (1999). https://doi.org/10.1038/sj.onc.1203134.

[42] C.D. Woodworth, L.P. Disfendorf, D.F. Jette, A. Mohammed, M.A. Moses, S.A. Searleman, D.A. Stevens, K.M. Wilton, S. Mondal, Inhibition of the epidermal growth factor receptor by erlotinib prevents immortalization of human cervical cells by Human Papillomavirus type 16, Virology. 421 (2011) 19–27. https://doi.org/10.1016/j.virol.2011.09.014.

[43] L. Zhang, J. Wu, M.T. Ling, L. Zhao, K.N. Zhao, The role of the PI3K/Akt/mTOR signalling pathway in human cancers induced by infection with human papillomaviruses, Mol. Cancer. 14 (2015) 1–13. https://doi.org/10.1186/s12943-015-0361-x.

[44] D. Pim, P. Massimi, S.M. Dilworth, L. Banks, Activation of the protein kinase B pathway by the HPV-16 E7 oncoprotein occurs through a mechanism involving interaction with PP2A, Oncogene. (2005). https://doi.org/10.1038/sj.onc.1208935.

[45] O. Chakrabarti, K. Veeraraghavalu, V. Tergaonkar, Y. Liu, E.J. Androphy, M.A.

Stanley, S. Krishna, Human Papillomavirus Type 16 E6 Amino Acid 83 Variants Enhance E6-Mediated MAPK Signaling and Differentially Regulate Tumorigenesis by Notch Signaling and Oncogenic Ras, J. Virol. (2004). https://doi.org/10.1128/jvi.78.11.5934-5945.2004.

[46] K. Liu, J.C. Paik, B. Wang, F.T. Lin, W.C. Lin, Regulation of TopBP1 oligomerization by Akt/PKB for cell survival, EMBO J. 25 (2006) 4795–4807. https://doi.org/10.1038/sj.emboj.7601355.

[47] N. Dammes, D. Peer, Paving the Road for RNA Therapeutics, Trends Pharmacol. Sci. (2020). https://doi.org/10.1016/j.tips.2020.08.004.

[48] H. Chapoy-Villanueva, I. Martinez-Carlin, G. Lopez-Bernstein, A. Chavez-Reyes, Therapeutic silencing of HPV 16 E7 by systemic administration of siRNA-neutral DOPC nanoliposome in a murine cervical cancer model with obesity, J. B.U.ON. (2015).

[49] S.Y. Wu, A. Singhania, M. Burgess, L.N. Putral, C. Kirkpatrick, N.M. Davies, N.A.J. McMillan, Systemic delivery of E6/7 siRNA using novel lipidic particles and its application with cisplatin in cervical cancer mouse models, Gene Ther. (2011). https://doi.org/10.1038/gt.2010.113.

[50] H. Nishida, Y. Matsumoto, K. Kawana, R.J. Christie, M. Naito, B.S. Kim, K. Toh, H.S. Min, Y. Yi, Y. Matsumoto, H.J. Kim, K. Miyata, A. Taguchi, K. Tomio, A. Yamashita, T. Inoue, H. Nakamura, A. Fujimoto, M. Sato, M. Yoshida, K. Adachi, T. Arimoto, O. Wada-Hiraike, K. Oda, T. Nagamatsu, N. Nishiyama, K. Kataoka, Y. Osuga, T. Fujii, Systemic delivery of siRNA by actively targeted polyion complex micelles for silencing the E6 and E7 human papillomavirus oncogenes, J. Control. Release. (2016). https://doi.org/10.1016/j.jconrel.2016.03.016.

[51] J.O. Eloy, R. Petrilli, L.N.F. Trevizan, M. Chorilli, Immunoliposomes: A review on functionalization strategies and targets for drug delivery, Colloids Surfaces B Biointerfaces. (2017). https://doi.org/10.1016/j.colsurfb.2017.07.085.

[52] I.K. Kwon, S.C. Lee, B. Han, K. Park, Analysis on the current status of targeted drug delivery to tumors, J. Control. Release. (2012). https://doi.org/10.1016/j.jconrel.2012.07.010.

[53] D.B. Kirpotin, D.C. Drummond, Y. Shao, M.R. Shalaby, K. Hong, U.B. Nielsen, J.D. Marks, C.C. Benz, J.W. Park, Antibody targeting of long-circulating lipidic nanoparticles does not increase tumor localization but does increase internalization in animal models, Cancer Res. 66 (2006) 6732–6740. https://doi.org/10.1158/0008-5472.CAN-05-4199.

[54] H. Maeda, J. Wu, T. Sawa, Y. Matsumura, K. Hori, Tumor vascular permeability and the EPR effect in macromolecular therapeutics: A review, J. Control. Release. (2000). https://doi.org/10.1016/S0168-3659(99)00248-5.

[55] S. Marur, S. Li, A.J. Cmelak, M.L. Gillison, W.J. Zhao, R.L. Ferris, W.H. Westra, J. Gilbert, J.E. Bauman, L.I. Wagner, D.R. Trevarthen, J. Balkrishna, B.A. Murphy, N. Agrawal, A.D. Colevas, C.H. Chung, B. Burtness, E1308: Phase II trial of induction chemotherapy followed by reduced-dose radiation and weekly cetuximab in patients with HPV-associated resectable squamous cell carcinoma of the oropharynx- ECOG-ACRIN cancer research group, J. Clin. Oncol. 35 (2017) 490–497. https://doi.org/10.1200/JCO.2016.68.3300.

[56] M.L. Gillison, A.M. Trotti, J. Harris, A. Eisbruch, P.M. Harari, D.J. Adelstein, E.M. Sturgis, B. Burtness, J.A. Ridge, J. Ringash, J. Galvin, M. Yao, S.A. Koyfman, D.M. Blakaj, M.A. Razaq, A.D. Colevas, J.J. Beitler, C.U. Jones, N.E. Dunlap, S.A. Seaward, S. Spencer, T.J. Galloway, J. Phan, J.J. Dignam, Q.T. Le, Radiotherapy plus cetuximab or cisplatin in human papillomavirus-positive oropharyngeal cancer (NRG Oncology RTOG 1016): a randomised, multicentre, non-inferiority trial, Lancet. 393 (2019) 40–50. https://doi.org/10.1016/S0140-6736(18)32779-X.

Table 1. Characterization of LNPs by Dynamic Light Scattering and ζ-Potential Measurements.

	uncoated LNPs	**iso-LNPs**	**tLNPs**
Hydrodynamic diameter [d,nm]	67 ± 6.4	95 ± 6.3	89 ± 7.6
Polydispersity index	0.11 ± 0.05	0.18 ± 0.09	0.13 ± 0.07

Z-potential [mV]	-3.02 ± 0.64	-3.50 ± 0.33	-5.04 ± 0.71

Data represent mean ± SD of six independent preparations

Fig. 1. HPV E6/E7 silencing suppresses cell proliferation and restores p53 in HPV-positive HNC cells. **A**, Detection of HPV E6/E7 in HPV16-positive HNC cell lines: 2A3, UMSCC-104 and UPCI:SCC090 by RT-PCR and western blot analysis. **B**, Target gene expression in three HPV positive cell lines 48h after siE6 treatment compared to scrambled control siRNA (siNC), measured by RT-PCR. Data are representative of three independent experiments, two-tailed Student's t-test, **, p<0.005, ****, p<0.00005. **C**, Viability 72h after siE6 treatment compared to siNC. Results are mean ± SD from three six-plicates experiments, two-tailed Student's t-test, *, p<0.05, **, p<0.005, ****, p<0.00005. **D**, Immunoblotting for E7 and p53 72h after treatment with siE6 or siNC. GAPDH was used as a loading control. Numbers indicate p53/GAPDH and E7/GAPDH ratios, as determined by densitometric analysis.

Fig. 2. EGFR coating mediates tLNPs binding to HNC cells without impeding ultra-structure of the LNPs. **A**, Anti-EGFR antibodies (AF647) binding (at 4 °C) and internalizing into UMSCC-104 cells when incubated at 37 °C. **B,** Schematic diagram of the production process of siRNA-loaded tLNPs using ASSET technology. ASSET, expressed in the E. coli periplasm anchored by lipidation to the inner membrane, is purified in micelles and inserted into the LNPs which are then coated with mAbs. Adopted with permission from Veiga *et al*, *Adv Drug Deliv Rev* 2020.[38] **C**, Representative transmission electron microscopy (TEM) images of uncoated LNPs (left) and tLNPs (right), 100nm scale bar. **D**, Binding to UMSCC-104 cells of tLNPs (red) or iso-LNPs (blue) encapsulating Cy5-labelled siRNA.

Fig. 3. tLNPs-siE6 suppress E6 and E7 expression and lead to apoptotic cell death of HPV-positive HNSCC cells. **A**, Confocal images of untreated UMSCC-104 cells (Mock) or tLNPs-siE6-treated cells, stained for E7 (top, green) and Rb (bottom, green) 72h after treatment. Nuclei were stained with DAPI (blue). **B**, Relative E6 expression in UMSCC-104 cells 48h after different LNPs-siRNA treatments, as measured by RT-PCR. Data represent the mean±SD of three independent experiments, one-way ANOVA, *p<0.05. **C,** Immunoblotting for E7 72h after treatment. GAPDH

served as a loading control. **D**, Annexin V/PI staining of UMSCC-104 and FaDu cells 96h after treatment with siNC or siE6 encapsulated in uncoated, iso- or tLNPs. Results are mean ±SD of three independent experiments, 2-way ANOVA, *** $p<0.0005$.

Fig. 4. Biodistribution and tumor accumulation of tLNPs and iso-LNPs in xenograft tumor-bearing mice. **A**, Representative IVIS images of mCherry signal (tumor cells) and Cy5 signal (LNPs) in tumor bearing mice 2h post-injection with either iso-LNPs or tLNPs. In the images of Cy5 fluorescence the tumors are marked by dashed circles. **B-C,** Biodistribution of Cy5-labelled iso-LNPs and tLNPs at 4h (B) and 24h (C) post-injection (n=6 mice per group). **D-E**, Representative IVIS images of the tumors harvested from mice at 4h (D) and 24h (E) after iv LNPs administration, and quantification of Cy5 fluorescence intensity by living image software comparing iso-LNPs *vs*. tLNPs tumor uptake (n=6 mice per time point). NS, not significant. Data (**B-E**) are representative of two independent experiments per time point (4h and 24h).

Fig. 5. Active targeting enhances LNPs uptake by tumor cells. Tumors were excised 4h post injection of iso-LNPs or tLNPs, and cryosections stained for EGFR (green), to mark tumor cell surface, and DAPI (blue) to label nuclei. LNPs were visualized by Cy5 fluorescence (magenta). **A-B** tLNPs were found in close association with the surface of tumor cells or taken up by tumor cells (white arrows). In contrast, iso-LNPs were mostly in the interstitial matrix (orange arrows) as identified by dense areas of smaller-nuclei cells compared to tumor cells (C-D). Images are representative of two independent experiments.

Fig. 6. αEGFR tLNP siE6 mediates therapeutic gene silencing in a xenograft HPV-positive HNC mouse model. **A,** UMSCC-104 cells were subcutaneously inoculated in FoxN1 nude mice. After tumors had reached approximately 50 mm^3, mice were intravenously injected with tLNPs or iso-LNPs encapsulating siE6 or siNC on days 12,15,19,22,25 and 28, n=10 mice/group. Data are presented as mean ± SEM; one-way ANOVA, * $p<0.05$, ** $p<0.005$ tLNPs-siE6 *vs*. iso-LNPs-siNC **B**, *in vivo* E6/E7 silencing in xenograft tumors by either tLNPs or iso-LNPs encapsulating siE6 or siNC, n=5 mice/group. Data are presented as interquartile range (IQR) with a median center line and minimum to maximum error bars; one-way ANOVA, * $p<0.05$, ***$p<0.0005$, ****$p<0.00005$ **C,** H&E staining (scale bar, 200μm), immunohistochemical staining of P16 (scale bar, 100 μm) and TUNEL staining of tumor tissues. **D**, Statistical analysis (mean ± SD) of the percentage of apoptotic cells in tumor tissues as determined by TUNEL assay (representative images in panel D). A total of 3 fields from each

treatment group were counted. One-way ANOVA, ** p<0.005. Data (**A-D**) are representative of two independent experiments.

Graphical abstract